A General Framework for Development and Data Analysis of Competitive High-Throughput Screens for Small-Molecule Inhibitors of Protein−Protein Interactions by Fluorescence Polarization†

Michael H. A. Roehrl,‡,§ Julia Y. Wang,|| and Gerhard Wagner*,‡

Department of Biological Chemistry and Molecular Pharmacology, Harvard Medical School, 240 Longwood Avenue, Channing Laboratory, Department of Medicine, Brigham and Women's Hospital, 181 Longwood Avenue, and Graduate Program in the Biological and Biomedical Sciences, Division of Medical Sciences, Faculty of Arts and Sciences, Harvard University, 220 Longwood Avenue, Boston, Massachusetts 02115

Received August 16, 2004; Revised Manuscript Received October 15, 2004

ABSTRACT: Equilibrium binding experiments are widely used for the accurate characterization of binding and competitive binding behavior in biological systems. Modern high-throughput discovery efforts in chemical biology rely heavily upon this principle. Here, we derive exact analytical expressions for general competitive binding models which can also explain a commonly encountered phenomenon in these types of experiments, anticooperative incomplete displacement. We explore the effects of nonspecific binding behavior and parameter misestimation. All expressions are derived in terms of total concentrations determined *a priori*. We discuss a general framework for high-throughput screening assays based on fluorescence polarization and strategies for assay development, sensitivity regimes, data quality control, analysis, and ranking. Theoretical findings are visualized by simulations using realistic parameter sets. Our results are the basis for the discovery of small-molecule inhibitors of the protein−protein interaction between human calcineurin and NFAT transcription factors, as discussed in the subsequent paper (*31*).

Large complex networks of interactions between biomacromolecules are at the very center of biological and biochemical processes in living organisms (*1*−*5*). In particular, protein−protein and protein−ligand interactions, spanning a wide range of affinities, are a focus of great interest for fundamental biological (*6*−*8*) and biophysical (*9*, *10*) investigation and as targets for drug development and pharmacological intervention (*11*, *12*). Recent advances in chemical biology and high-throughput (HTP)[1] screening (*13*−*15*) have introduced the use of structurally diverse small organic molecules for the targeted manipulation of protein interactions (*16*, *17*). For one case of enzyme−substrate interactions, we have previously defined this concept as substrate-selective enzyme inhibition (SSEI) (*18*), which entails the inhibition of a specific enzyme−substrate docking site with the preservation of catalytic activity toward other substrates.

Fluorescence polarization (FP) is one of the most sensitive, robust, and widely used HTP methods for the study of protein interactions and drug discovery (*19*−*22*). When a fluorophore is excited with polarized light, the emitted light is also polarized. The degree of polarization is a function of molecular properties, most specifically, Brownian molecular rotation, and, hence, can serve as a sensitive molecular sensor. HTP FP assays usually detect changes in polarization caused by changes in the molecular mass of the labeled species. Such examples include enzymatic release of the free fluorophore (*23*) or displacement of molecular complexes (*24*).

FP assays are typically designed as competitive equilibrium binding assays. For algebraic simplicity, equilibrium binding is described in most textbooks in terms of effective concentrations of the various molecular species involved (*25*−*28*), but not in terms of *a priori* known absolute input concentrations. This makes the direct use of the equations impractical for data fitting and parameter estimation. An exact analytical treatment of competitive binding has, to our knowledge, not previously been applied to FP experiments. Instead, numerical approximations are more commonly used (*29*). Only rarely has an analytical approach been attempted, and then limited, however, to detection methods other than FP (*30*). Furthermore, incomplete competitive displacement, as described by a four-state model, has, to the best of our knowledge, not been analyzed in this context before. Moreover, there are numerous examples in the literature in which FP data have been fitted to incorrect relationships, wrongly assuming a linear superposition principle for polarization. Anisotropy should have been used instead (*vide infra*), or the correct nonlinear superposition principle should have been applied.

† G.W. acknowledges support from the NIH (Grants GM038608 and AI037581). Purchase and maintenance of equipment used for this research were supported by NIH Grants RR000995 and GM047467.

* To whom correspondence should be addressed: Department of Biological Chemistry and Molecular Pharmacology, Building C1, Harvard Medical School, 240 Longwood Ave., Boston, MA 02115. Phone: (617) 432-3213. Fax: (617) 432-4383. E-mail: gerhard_wagner@hms.harvard.edu.

‡ Harvard Medical School.

§ Harvard University.

|| Brigham and Women's Hospital.

[1] Abbreviations: FP, fluorescence polarization; HTP, high-throughput; NFAT, nuclear factor of activated T cells.

10.1021/bi048233g CCC: $27.50
Published on Web 11/26/2004

We feel that a comprehensive investigation of binding scenarios and a road map for the successful design of HTP FP assays are timely and useful. In this and a subsequent paper (*31*), we provide further details on our work on the selective disruption of the NFAT−calcineurin complex (*31*). In the paper presented here, we discuss the theoretical framework of screening assays based on FP and strategies for HTP assay development, sensitivity regimes, data quality control, analysis, and ranking. The results are general and widely applicable to equilibrium competition studies. We also provide numerical simulations for visually exploring the theoretical results and a procedural flowchart for the practical realization of HTP FP assay projects. Our results are the basis for the discovery of novel NFAT-directed small-molecule inhibitors of human calcineurin (*18*, *31*).

1. THEORY

The following presentation focuses on direct binding of one ligand or competitive binding of two ligands to a binding partner under equilibrium conditions. We will study both complete and incomplete competitive binding and extend our models to account for nonspecific binding effects.

1.1. Direct Binding. In FP assays, a fluorescently labeled ligand, L_S,[2] binds to an unlabeled receptor, R. If one does not account for potential nonspecific binding events, this simple interaction is described by eqs 1−4 and is illustrated in Figure 1A.

$$K_{D1} = \frac{R L_S}{RL_S} \tag{1}$$

$$R_T = R + RL_S \tag{2}$$

$$L_{ST} = L_S + RL_S \tag{3}$$

$$F_{SB} = 1 - \frac{L_S}{L_{ST}} \tag{4}$$

R, L_S, and RL_S denote free (unbound) concentrations of the receptor, labeled ligand, and labeled ligand−receptor complex, respectively. K_{D1} is the dissociation constant of the interaction. R_T and L_{ST} are total input concentrations of the receptor and labeled ligand, respectively, and F_{SB} represents the fraction of bound labeled ligand. To obtain physically meaningful results, we assume throughout the paper that all concentrations and dissociation constants are non-negatively finite.

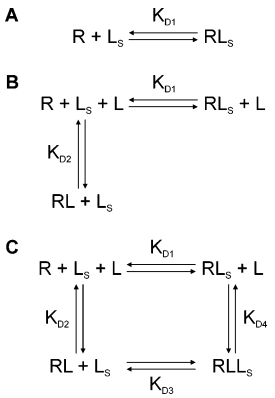

FIGURE 1: (A) Direct binding model. (B) Complete competitive binding model. (C) Incomplete competitive binding model (four-state model).

In experiments with fluorescently labeled ligands, the total concentration of labeled ligand, L_{ST}, is typically kept constant and the relationship between R_T (independent variable) and F_{SB} (dependent variable) is measured (*vide infra*) to extract an estimate of K_{D1}. Solving eqs 1−4 for R_T and eliminating R, L_S, and RL_S, we obtain eq 5.

$$R_T = \frac{-L_{ST}F_{SB}^2 + (K_{D1} + L_{ST})F_{SB}}{1 - F_{SB}} \tag{5}$$

We note that eq 5 is quadratic in F_{SB}. Solving eqs 1−4 for F_{SB} analogously, we find the well-known eq 6. Note that only the given root represents a physical solution.

$$F_{SB} = \frac{K_{D1} + L_{ST} + R_T - \sqrt{(K_{D1} + L_{ST} + R_T)^2 - 4L_{ST}R_T}}{2L_{ST}} \tag{6}$$

The dependence of F_{SB} on R_T and K_{D1} is simulated and discussed in section 2.1 of this paper (Figure 2A, *vide infra*).

We can model nonspecific immobilization of the labeled ligand by introducing a dimensionless, non-negative parameter, N_S, and modifying eq 3 to give eq 7.

$$L_{ST} = L_S + RL_S + N_S L_S \tag{7}$$

Here, it is assumed that, for typically available ligand concentrations, nonspecific binding is nonsaturable and linearly proportional to the free labeled ligand concentration (*30*). Examples of such interactions could include nonspecific sites on the receptor, other reaction buffer components, or the reaction compartment. Solving individually for R_T and F_{SB}, we obtain eqs 8 and 9. Like eq 6, eq 9 represents the physical solution.

$$R_T = \frac{-aF_{SB}^2 + b_1F_{SB} - (K_{D1} + L_{ST})N_S}{1 - F_{SB}} \tag{8}$$

with

$$a = L_{ST} + N_S L_{ST}$$

[2] Definitions of repeatedly used variables (Note that in this paper complexes are printed in regular font, not italics.): R_T, total receptor concentration; R, concentration of the free receptor; L_{ST}, total concentration of the labeled ligand (probe); L_S, concentration of the free labeled ligand (probe); L_T, total concentration of the unlabeled ligand (competitor); L, concentration of the free unlabeled ligand (competitor); RL_S, concentration of the binary complex of the receptor and labeled ligand (probe); RL, concentration of the binary complex of the receptor and unlabeled ligand (competitor); RLL_S, concentration of the ternary complex of the receptor, unlabeled ligand (competitor), and labeled ligand (probe); K_{D1}, dissociation constant of the interaction between R and L_S (probe); K_{D2}, dissociation constant of the interaction between R and L (competitor); K_{D3}, dissociation constant of the interaction between the RL complex and L_S; F_{SB}, fraction of bound labeled ligand (probe); N_S, parameter for nonspecific binding of the labeled ligand (probe); N, parameter for nonspecific binding of the unlabeled ligand (competitor); $I^{=}$, fluorescence intensity parallel to the plane of exciting light; $I^{\perp}$, fluorescence intensity perpendicular to the plane of exciting light; A, anisotropy; κ, angle between absorption and emission dipoles; λ, angle associated with local motion of the fluorescent moiety; τ_F, fluorescence lifetime of the fluorophore; τ_C, rotational correlation time of the observed species; Q, ratio of fluorescence intensities of bound and free species.

and

$$b_1 = (1 + N_S)K_{D1} + L_{ST} + 2N_S L_{ST}$$

$$F_{SB} = \frac{K_{D1} + L_{ST} + R_T + (K_{D1} + 2L_{ST})N_S - \sqrt{c}}{2(1 + N_S)L_{ST}} \quad (9)$$

with

$$c = (1 + N_S)^2 K_{D1}{}^2 + 2(1 + N_S)(L_{ST} + R_T)K_{D1} + (L_{ST} - R_T)^2$$

In analogy to eq 5, eq 8 is quadratic in F_{SB}. When $N_S = 0$, eqs 8 and 9 become equivalent to eqs 5 and 6, respectively, and we recover the purely specific binding case. Since F_{SB} is closely related to the spectroscopic readout of anisotropy in FP as a function of R_T (see section 1.4), data can be directly fitted using eq 6 or 9 (i.e., the measured dependent variable is expressed as a function of the independent input variable).

To perform accurate competition experiments, we will in general only pursue labeled ligands that do not display significant nonspecific binding behavior, i.e., for which we find $N_S = 0$. An estimate of the contribution of N_S originating from nonspecific binding to the reaction compartment or its components other than the receptor may be obtained by measuring the anisotropy of the labeled ligand in the absence of receptor. If this value is significantly greater than that and is consistent with the type of fluorphore used and the size of the labeled ligand (see section 1.4 and ref *31*), one can conclude that $N_S > 0$. In fact, when $R_T = 0$ we find eq 10, from which N_S can be directly determined.

$$F_{SB}{}^{(R_T=0)} = \frac{N_S}{1 + N_S} \quad (10)$$

Let us finally consider the effect on the estimate of K_{D1}, if it were falsely assumed that $N_S = 0$, even though N_S is in reality greater than zero. One would then (incorrectly) conclude that $F_{SB} = 0$ when $R_T = 0$. Using eq 10, the assumed fraction of the bound labeled ligand, F_{SBA}, and the true fraction, F_{SB}, are then related by eq 11.

$$F_{SBA} = (1 + N_S)F_{SB} - N_S \quad (11)$$

Solving for R_T in analogy to eq 8, we obtain eq 12.

$$R_T = \frac{-aF_{SB}{}^2 + b_2 F_{SB} - \left(\frac{1}{1 + N_S}K_{D1A} + L_{ST}\right)N_S}{1 - F_{SB}} \quad (12)$$

with

$$a = L_{ST} + N_S L_{ST}$$

and

$$b_2 = K_{D1A} + L_{ST} + 2N_S L_{ST}$$

where K_{D1A} denotes the dissociation constant that would be obtained under the assumption $N_S = 0$. By direct comparison of eqs 8 and 12, we find that K_{D1A} is greater than the true value, K_{D1}, by a multiplicative factor of $1 + N_S$. Hence, K_{D1A} is always a robust upper bound estimate of the true dissociation constant; i.e., neglecting nonspecific effects will, at worst, introduce a conservative error and lead to overestimation of the dissociation constant. In section 2.1, numerical simulations illustrate these effects (Figure 2B, *vide infra*).

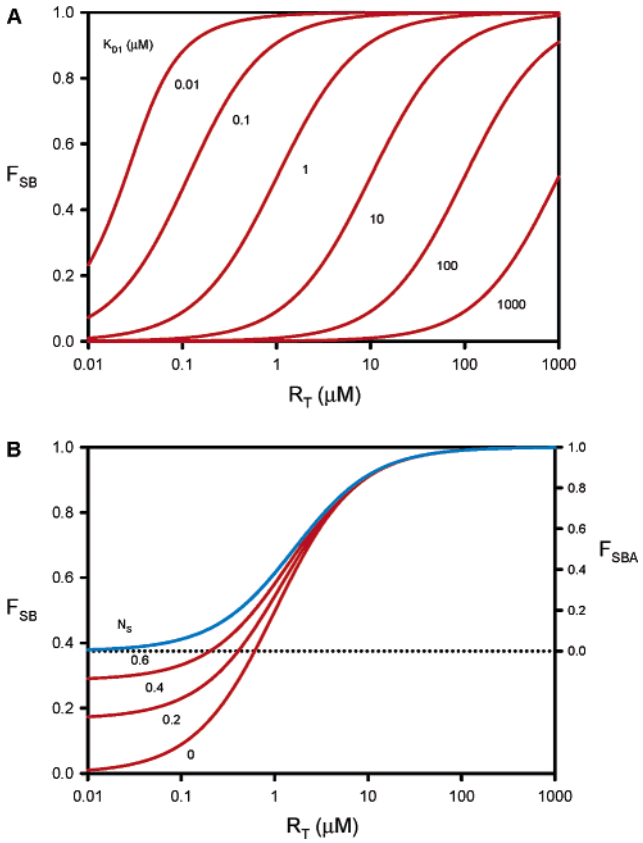

FIGURE 2: (A) Direct binding model without nonspecific effects (eq 9). (B) Direct binding model with nonspecific effects (eqs 9 and 11).

1.2. Complete Competitive Binding. In competitive FP assays, an unlabeled ligand, L, and a fluorescently labeled ligand, L_S, compete for binding to an unlabeled receptor, R. Complete competitive binding means here that binding of labeled and unlabeled ligands is mutually exclusive. Not accounting for potential nonspecific binding events, this interaction scheme is described by eqs 1, 3, 4, and 13−15 and is illustrated in Figure 1B.

$$K_{D2} = \frac{RL}{RL} \quad (13)$$

$$R_T = R + RL_S + RL \quad (14)$$

$$L_T = L + RL \quad (15)$$

L, RL, and L_T denote free unlabeled ligand, unlabeled ligand−receptor complex, and total unlabeled ligand input concentrations, respectively. K_{D2} is the dissociation constant of the interaction between L and R. In all competitive types of experiments, complete or incomplete (*vide infra*), we further assume $R_T > L_{ST}$. Otherwise, considerable amounts of free labeled ligand would always be present and interfere with measurements.

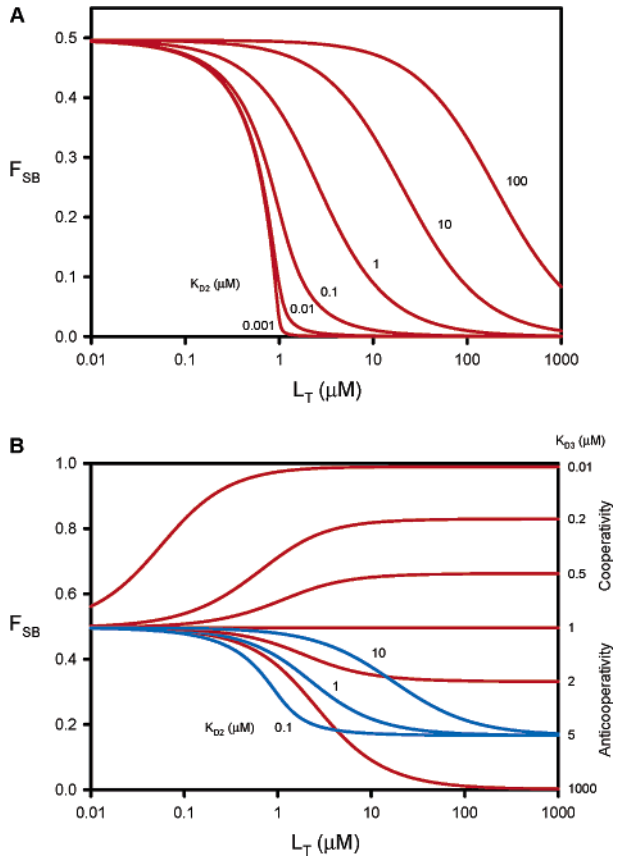

FIGURE 3: (A) Complete competitive binding model without nonspecific effects (eq 17). (B) Incomplete competitive binding model without nonspecific effects (eq 27).

Ways and means to the precise determination of K_{D1} are the ultimate experimental goal of competitive binding assays (*18*, *31*). Experimentally, R_T and L_{ST} are typically kept constant, and the relationship between L_T (independent variable) and F_{SB} (dependent variable) is analyzed to extract an estimate of K_{D2}. K_{D1} must have been previously obtained from a direct binding experiment (see section 1.1), as is typically done when a binding assay is developed. Solving the six equations for L_T and eliminating R, L_S, RL_S, L, and RL, we obtain eq 16.

$$L_T = \frac{[(K_{D1} - K_{D2})F_{SB} + K_{D2}][L_{ST}F_{SB}^{\ 2} - (K_{D1} + L_{ST} + R_T)F_{SB} + R_T]}{(1 - F_{SB})F_{SB}K_{D1}} \quad (16)$$

We note that eq 16 is cubic in F_{SB}. Solving for F_{SB} analogously yields a unique physically meaningful root expressed by eq 17 (*30*).

$$F_{SB} = \frac{2\sqrt{(d^2 - 3e)}\cos(\theta/3) - d}{3K_{D1} + 2\sqrt{(d^2 - 3e)}\cos(\theta/3) - d} \quad (17)$$

with

$$d = K_{D1} + K_{D2} + L_{ST} + L_T - R_T$$

$$e = (L_T - R_T)K_{D1} + (L_{ST} - R_T)K_{D2} + K_{D1}K_{D2}$$

$$f = -K_{D1}K_{D2}R_T$$

and

$$\theta = \arccos\left[\frac{-2d^3 + 9de - 27f}{2\sqrt{(d^2 - 3e)^3}}\right]$$

The dependence of F_{SB} on L_T and K_{D2} is numerically simulated and discussed in section 2.2 (Figure 3A, *vide infra*).

In analogy to eq 7, we can model nonspecific immobilization of the unlabeled ligand by introducing a dimensionless, non-negative parameter, N, and modifying eq 15 to give eq 18.

$$L_T = L + RL + NL \quad (18)$$

However, as laid out in section 1.1, we will not accommodate here nonspecific binding of the labeled ligand, since such molecules should be avoided in competitive experiments. Solving eqs 1, 3, 4, 13, 14, and 18 for L_T, we obtain eq 19.

$$L_T = \{\{[K_{D1} - (1 + N)K_{D2}]F_{SB} + (1 + N)K_{D2}\}[L_{ST}F_{SB}^{\ 2} - (K_{D1} + L_{ST} + R_T)F_{SB} + R_T]\}/[(1 - F_{SB})F_{SB}K_{D1}] \quad (19)$$

We note that eq 19 is cubic in F_{SB}. Alternatively, we can solve eqs 1, 3, 13, 14, and 18 to obtain eq 20, a cubic polynomial in R.

$$R^3 + gR^2 + hR + i = 0 \quad (20)$$

with

$$g = K_{D1} + (1 + N)K_{D2} + L_{ST} + L_T - R_T$$

$$h = (L_T - R_T)K_{D1} + (1 + N)(L_{ST} - R_T)K_{D2} + (1 + N)K_{D1}K_{D2}$$

$$i = -(1 + N)K_{D1}K_{D2}R_T$$

In analogy to eq 17 and also using eq 4, we can solve for F_{SB} and obtain eq 21.

$$F_{SB} = \frac{2\sqrt{(g^2 - 3h)}\cos(\xi/3) - g}{3K_{D1} + 2\sqrt{(g^2 - 3h)}\cos(\xi/3) - g} \quad (21)$$

with

$$\xi = \arccos\left[\frac{-2g^3 + 9gh - 27i}{2\sqrt{(g^2 - 3h)^3}}\right]$$

By a comparison of eq 16 with eq 19 and eq 17 with eq 21, it can be seen that nonspecific binding of unlabeled ligand is formally equivalent to a multiplicative increase in the specific dissociation constant K_{D2} by a factor of $1 + N$. The notable consequence is that competitive binding experiments *per se* cannot directly separate the two effects. In the absence of an independent estimate of N, K_{D2} fitted according to eq 16 or 17 provides, however, a reliable upper limit for the specific dissociation constant.

1.3. Incomplete Competitive Binding. We find from simulations (see section 2) that the complete competitive

binding model derived above predicts invariably $F_{SB} \rightarrow 0$ in the limit of increasingly large L_T; i.e., labeled ligand can always be completely displaced from the receptor by an excess of the unlabeled ligand. We have found experimentally, however, that a significant number of small-molecule ligands identified in HTP screens are not able to displace the labeled ligand entirely and are characterized by an asymptotic limit of F_{SB} that is greater than zero (*31*, *32*). We introduce here an incomplete competitive binding model (four-state model) that can account for this phenomenon. Not considering potential nonspecific binding events, this interaction scheme is described by eqs 1, 4, 13, and 22−26 and is illustrated in Figure 1C.

$$K_{D3} = \frac{R\,L L_S}{RLL_S} \tag{22}$$

$$K_{D4} = \frac{K_{D2}K_{D3}}{K_{D1}} = \frac{RL_S\,L}{RLL_S} \tag{23}$$

$$R_T = R + RL_S + RL + RLL_S \tag{24}$$

$$L_{ST} = L_S + RL_S + RLL_S \tag{25}$$

$$L_T = L + RL + RLL_S \tag{26}$$

RLL_S denotes the concentration of the isostoichiometric ternary complex of the labeled ligand, unlabeled ligand, and receptor. K_{D3} and K_{D4} are dissociation constants. For thermodynamic reasons, the model only permits three independent dissociation constants. We can thus express K_{D4} as a function of the other three (eq 23). Solving the eight equations for L_T while eliminating R, L_S, RL_S, L, RL, and RLL_S yields eq 27 ($K_{D3} \neq K_{D1}$).

$$L_T = \frac{j\{[kl - (1 - F_{SB})K_{D2}K_{D3}]K_{D1} + (1 - F_{SB})K_{D2}K_{D3}^2\}}{k(1 - F_{SB})(K_{D1} - K_{D3})K_{D1}} \tag{27}$$

with

$$j = L_{ST}F_{SB}^2 - (K_{D1} + L_{ST} + R_T)F_{SB} + R_T$$

$$k = L_{ST}F_{SB}^2 - (K_{D3} + L_{ST} + R_T)F_{SB} + R_T$$

and

$$l = L_{ST}F_{SB} - K_{D3} - L_{ST}$$

We note that eq 27 is a fifth-degree polynomial in F_{SB}, and therefore, an explicit solution for F_{SB} cannot generally be given. Nevertheless, numerical methods allow efficient fitting of experimental data to eq 27 (*31*). We shall note that F_{SB} has a bounded limit for $L_T \rightarrow \infty$, as given by eq 28.

$$\lim_{L_T \rightarrow \infty} F_{SB} = \frac{K_{D3} + L_{ST} + R_T - \sqrt{(K_{D3} + L_{ST} + R_T)^2 - 4L_{ST}R_T}}{2L_{ST}} \tag{28}$$

Depending on the value of K_{D3}, this limit ranges from 0 to 1 and reflects asymptotically incomplete displacement. In section 2.3 (Figure 3B, *vide infra*), the dependence of F_{SB} on L_T, K_{D2}, and K_{D3} is discussed and graphically illustrated by numerical simulations.

We can model nonspecific binding effects of the unlabeled ligand by modifying eq 26 to give eq 29.

$$L_T = L + RL + RLL_S + NL \tag{29}$$

Solving for L_T ($K_{D3} \neq K_{D1}$), we find eq 30, which is identical to eq 27, except that K_{D2} is replaced everywhere by $(1 + N)K_{D2}$.

$$L_T = \frac{j\{[kl - (1 - F_{SB})(1 + N)K_{D2}K_{D3}]K_{D1} + (1 - F_{SB})(1 + N)K_{D2}K_{D3}^2\}}{k(1 - F_{SB})(K_{D1} - K_{D3})K_{D1}} \tag{30}$$

Just like in the complete competitive binding model, we see that it is not possible to separate specific from nonspecific effects based on competitive experiments alone. Equations 19, 21, and 30 can be useful, if an estimate of N has been obtained independently, e.g., from a direct binding experiment (see section 1.1). Alternatively, if nonspecific effects are neglected, K_{D2} always provides a robust upper bound estimate of the true dissociation constant.

From simulations (see section 2.3), we find that, if $K_{D3} > K_{D1}$, we observe displacement of bound L_S (i.e., decrease in F_{SB}) for an increase in L_T (anticooperativity). Conversely, if $K_{D3} < K_{D1}$, we observe an increase in bound L_S (i.e., increase in F_{SB}) for an increase in L_T (cooperativity). In both cases, F_{SB} converges to a precise, bounded limit (eq 28). Let us finally consider the special case where $K_{D3} = K_{D1}$. Under this condition, the system of eqs 1, 4, 13, 22−25, and 29 can be solved explicitly for F_{SB}, while eliminating R, L_S, RL_S, L, RL, and RLL_S. The result is identical to eq 6. Since eq 6 is independent of L_T, we find that F_{SB} remains constant, independent of the amount of unlabeled ligand present. This is because, under these particular conditions, labeled and unlabeled ligands do not influence each other's binding equilibria with the receptor.

1.4. Relationships between FP Observables and Binding States. When a fluorophore is excited with polarized light, the emitted light is also polarized as a function of fluorescence lifetime and rotational diffusion. The corresponding FP observables are typically the fluorescence intensities parallel, $I^{=}$, and perpendicular, $I^{\perp}$, to the plane of exciting light. We assume in the following that the relative sensitivities of the two acquisition channels have been calibrated, a procedure commonly termed G factor correction (*21*). The values for polarization, P, and anisotropy, A, are then defined by eqs 31 and 32.

$$P = \frac{I^{=} - I^{\perp}}{I^{=} + I^{\perp}} \tag{31}$$

$$A = \frac{I^{=} - I^{\perp}}{I^{=} + 2I^{\perp}} \tag{32}$$

Both P and A are in principle unitless, but polarization is sometimes given in the literature as 1000 P in units of mP ("millipolarization"). We will see that for algebraic simplicity it is preferable to work with anisotropy. The two parameters

are related by the nonlinear relationship given in eq 33.

$$A = \frac{2P}{3 - P} \tag{33}$$

The anisotropy of a rigid system that is not subject to rotational diffusion is called the limiting anisotropy, A_0, and is given by eq 34, where κ is the angle between absorption and emission transition dipoles (*33*).

$$A_0 = \frac{3\cos^2\kappa - 1}{5} \tag{34}$$

If the fluorescent probe retains residual flexibility with respect to a covalently tethered, completely immobilized binding epitope (e.g., a peptide), A_0 can be approximated by eq 35, where λ represents the angle associated with local motion (*22*).

$$A_0 = \left(\frac{3\cos^2\kappa - 1}{5}\right)\left(\frac{3\cos^2\lambda - 1}{2}\right) \tag{35}$$

It can be seen that the maximum value of A_0 is 0.4. A is related to A_0, the fluorescence lifetime of the fluorophore, τ_F, and the rotational correlation time of the observed molecule, τ_C, according to eq 36.

$$A = \left(1 + \frac{\tau_F}{\tau_C}\right)^{-1} \times A_0 \tag{36}$$

where τ_F is characteristic for the type of fluorophore used, e.g., ~4 ns for fluorescein-based labels. τ_C can be estimated from eq 37, if we assume first-order spherical solution geometry of the labeled species.

$$\tau_C = \frac{\eta M V_{HS}}{RT} \approx (4.1 \times 10^{-13} \times M) s Da^{-1} \tag{37}$$

For this estimate at 293.0 K, the aqueous viscosity, η, is 0.010 g cm^{-1} s^{-1} (assumed to be solute-independent for dilute solutions), the hydrated specific volume, V_{HS}, is typically 1.0 cm^3/g for proteins, and the universal gas constant, R, is 8.314 J K^{-1} mol^{-1}. M denotes the molecular mass of the labeled species in Daltons. Sophisticated corrections for other geometries and more general estimation approaches have been developed (*31*, *34*, *35*).

Multicomponent mixtures are described by eq 38, where A_{OBS} is the total observed anisotropy, ϕ_m is the fractional fluorescence intensity (or quantum yield) of the mth component, and A_m is the anisotropy of the mth component.

$$A_{OBS} = \sum_m \phi_m A_m \tag{38}$$

with

$$\sum_m \phi_m = 1$$

The principal reason for the preferential use of A over P for quantitative analyses is that this simple linear superposition principle does not hold for P. It should be noted here that the literature is rich in examples documenting confusion over this fact (*23*, *24*, *36*−*38*).

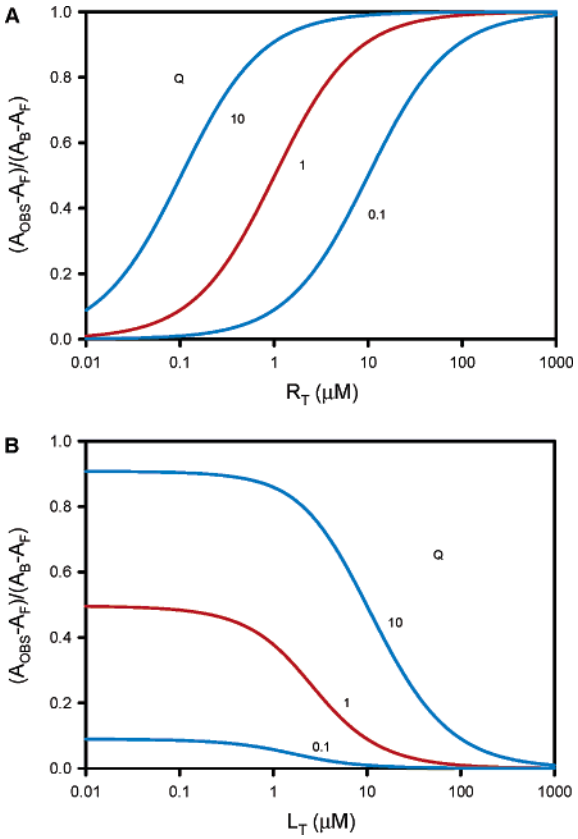

FIGURE 4: (A) Influence of Q on the observed anisotropy in the direct binding model (eqs 9 and 39). (B) Influence of Q on the observed anisotropy in the complete competitive binding model (eqs 17 and 39).

In the particular case of a mixture of two distinct species, e.g., free and bound labeled ligand (such as in direct or competitive FP binding experiments), A_{OBS} can be expressed as eq 39.

$$A_{OBS} = \frac{QF_{SB}A_B + (1 - F_{SB})A_F}{1 - (1 - Q)F_{SB}} \tag{39}$$

A_B and A_F denote anisotropies of bound and free species, respectively. Q is the ratio of fluorescence intensities (or quantum yields) of bound and free species measured under the same experimental conditions. In practice, Q is often found to be very close to 1, if the fluorophore is not directly involved in the binding event (*31*). A Q of <1 would, for example, mean that quenching of the fluorophore occurs upon binding. Solving eq 39 for F_{SB}, we find eq 40.

$$F_{SB} = \frac{A_{OBS} - A_F}{(A_B - A_{OBS})Q + A_{OBS} - A_F} \tag{40}$$

Equations 39 and 40 provide a direct link between the experimental observables in FP and the theoretical description of direct and competitive binding as explored in sections 1.1−1.3. Graphical illustrations of these relationships are provided in section 2.4 (Figure 4, *vide infra*).

1.5. Sensitivity of Competitive Binding Assays. The sensitivity, S, of a competitive binding assay can be defined as the change in the fraction of the bound labeled ligand (F_{SB}) relative to the change of the total unlabeled competitor (L_T), as shown in eq 41.

$$S = \left|\frac{dF_{SB}}{dL_T}\right| \tag{41}$$

where S is a function of K_{D1}, K_{D2}, L_{ST}, L_T, and R_T. We seek to identify sets of initial conditions defined by these parameters that maximize S. Thus, knowledge of the functional dependence of S on these parameters is crucial for designing and implementing optimal FP screening assays.

For the following considerations, we take the functional forms for L_T and F_{SB} from eqs 16 and 17, respectively. We define a function $f(L_T)$ according to the right side of eq 17 such that $F_{SB} = f(L_T)$. We note that $0 < f(L_T) < 1$ and that $f(L_T)$ is continuous and monotonically decreasing. For the inverse of f, f^{-1}, we find consequently that $L_T = f^{-1}(F_{SB})$, where $f^{-1}(F_{SB})$ is given by the right side of eq 16. The total derivatives of f and f^{-1} with respect to their arguments are related by the standard relation of eq 42.

$$\frac{d}{dL_T}[f(L_T)] = \left\{\frac{d}{dF_{SB}}[f^{-1}(F_{SB})]\right\}^{-1} \tag{42}$$

Both derivatives are negative. Hence, we seek a minimum of the derivative of f or, equivalently, a maximum of the derivative of f^{-1}. Since the left side of eq 42 is rather cumbersome to evaluate explicitly, we can make beneficial use of the right side of this relationship. We first solve eq 16 for R_T to obtain eq 43.

$$R_T = \frac{\{n[(1 - F_{SB})L_{ST} + K_{D1}] + (1 - F_{SB})K_{D1}L_T\}F_{SB}}{n(1 - F_{SB})} \tag{43}$$

with

$$n = (K_{D1} - K_{D2})F_{SB} + K_{D2}$$

Differentiating f^{-1} with respect to F_{SB} and then substituting R_T with the right side of eq 43 yields eq 44.

$$\frac{d}{dF_{SB}}[f^{-1}(F_{SB})] = -\frac{n^2[(1 - F_{SB})^2L_{ST} + K_{D1}] + (1 - F_{SB})^2K_{D1}K_{D2}L_T}{n(1 - F_{SB})^2F_{SB}K_{D1}} \tag{44}$$

A necessary condition for a maximum of $(d/dF_{SB})[f^{-1}(F_{SB})]$ is then given by eq 45.

$$\frac{d^2}{dF_{SB}^2}[f^{-1}(F_{SB})] = 0 \tag{45}$$

Direct computation leads to eq 46 and provides the desired optimality criterion for K_{D1}, K_{D2}, L_{ST}, L_T, F_{SB}, and thence R_T via eq 43.

$$[(K_{D1} - K_{D2})F_{SB} + K_{D2}]^2\{[2(K_{D1} - K_{D2})F_{SB}^2 + 3K_{D2}F_{SB} - K_{D2}]K_{D1} - (1 - F_{SB})^3K_{D2}L_{ST}\} - (1 - F_{SB})^3[2(K_{D1} - K_{D2})F_{SB} + K_{D2}]K_{D1}K_{D2}L_T = 0 \tag{46}$$

Equation 46 is a fifth-degree polynomial in F_{SB}. In practice, K_{D1} and L_{ST} are given by the assay specifications, and L_T is set to zero to evaluate the initial competitive sensitivity. Optimal values of F_{SB} (and R_T) are then obtained by numerically solving eq 46 for those values of K_{D2}, for which assay sensitivity is to be maximized (*31*). The advantage of this procedure is that a competitive assay may be *a priori* optimized for a desired target range of expected competitor dissociation constants. Section 2.5 illustrates the above equations by numerical simulations based on conditions that are typically encountered in practice (Figure 5, *vide infra*).

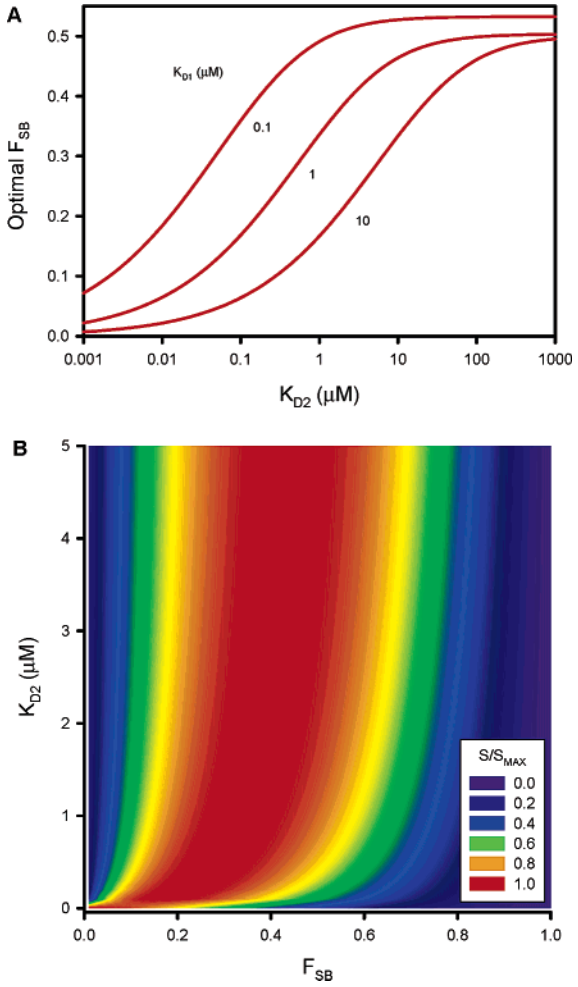

FIGURE 5: (A) Optimal F_{SB} as a function of K_{D2} (eq 46). (B) Normalized assay sensitivity, S/S_{MAX}, as a function of F_{SB} and K_{D2} (eqs 41 and 44). S_{MAX} is the maximum of S for a specific value of K_{D2} (i.e., along the ordinate).

1.6. Assay Quality, Data Analysis, and Ranking Strategies. FP assay quality can be assessed by two parameters, signal-to-noise ratio (S/N) and Z' factor, as given by eqs 47 and 48 (*39*).

$$\text{S/N} = \frac{A_U - A_F}{\sqrt{\sigma_U^2 + \sigma_F^2}} \tag{47}$$

$$Z' = \frac{(A_U - A_F) - (3\sigma_U + 3\sigma_F)}{A_U - A_F} \tag{48}$$

where A_U and A_F denote the upper (i.e., at a given R_T) and lower/free (i.e., $R_T = 0$) mean anisotropy bounds under specific assay conditions (i.e., at given L_{ST} and K_{D1}) with associated standard deviations, σ_U and σ_F, respectively. The

Z' factor describes the normalized gap size between the three-standard deviation bands around average upper and lower anisotropies. Assays wherein $Z' > 0.5$ are considered excellent (*39*), as illustrated in the subsequent paper (*31*).

The primary goal of initial data analysis is to eliminate FP data from intrinsically fluorescent or quenching competitors. Since the value of $I^{=} + 2I^{\perp}$ is directly proportional to total fluorescence intensity of the sample, this can be achieved by statistically analyzing the distribution and removing potential outliers (*18*).

Subsequently, the results from a high-throughput screen need to be ranked numerically for the identification of the most potent and promising hits. To this end, we introduce four ranking functions, R_1-R_4. A_{OBS} denotes in the following the observed assay anisotropy for a specific competitor L. R_1 is a linearized change of anisotropy model defined by eq 49.

$$R_1 = \frac{A_{OBS} - A_U}{A_U - A_F} \times 100\% \tag{49}$$

R_2 is a σ deviation model based on eq 50.

$$R_2 = \frac{A_{OBS} - A_U}{\sigma_U} \tag{50}$$

R_3 provides a single-point estimate of the dissociation constant of the competitor−receptor complex, K_{D2}, as given by eq 51. As shown in the Supporting Information, this estmate is obtained by solving eqs 1, 3, 4, and 13−15 for K_{D2} and expressing F_{SB} in terms of known quantities via eqs 6 and 40. R_3 is likely the most robust parameter, since it also takes actual compound screening concentrations into account, and may allow comparisons even across different types of assays.

$$R_3 = \frac{[-L_{ST}F_{SB}^{\ 2} + (K_{D1} + L_{ST} - L_T + R_T)F_{SB} + L_T - R_T]F_{SB}K_{D1}}{(1 - F_{SB})[L_{ST}F_{SB}^{\ 2} - (K_{D1} + L_{ST} + R_T)F_{SB} + R_T]} \tag{51}$$

with

$$F_{SB} = [2(A_{OBS} - A_F)R_T]/\{[K_{D1} + L_{ST} - (1 - 2Q)R_T + \sqrt{o}]A_U - (K_{D1} + L_{ST} + R_T + \sqrt{o})A_F + 2(1 - Q)R_TA_{OBS}\}$$

and

$$o = (K_{D1} + L_{ST} + R_T)^2 - 4L_{ST}R_T$$

which, when $Q = 1$, simplifies to

$$F_{SB} = \frac{A_{OBS} - A_F}{A_U - A_F}\left(\frac{K_{D1} + L_{ST} + R_T - \sqrt{o}}{2L_{ST}}\right)$$

R_4 is a total fluorescence change model according to eq 52.

$$R_4 = \frac{I_{OBS} - I_{EXP}}{I_{EXP}} \times 100\% \tag{52}$$

with

$$I_{EXP} = \frac{[1 - (1 - Q)F_{SB}]I_M}{1 - (1 - Q)p}$$

and

$$p = \frac{K_{D1} + L_{ST} + R_T - \sqrt{(K_{D1} + L_{ST} + R_T)^2 - 4L_{ST}R_T}}{2L_{ST}}$$

which, when $Q = 1$, simplifies to

$$R_4 = \frac{I_{OBS} - I_M}{I_M} \times 100\%$$

I_{OBS} denotes the observed value of $I^{=} + 2I^{\perp}$ for a specific competitor L. I_{EXP} is the expected, Q-corrected value at a given F_{SB}, and I_M is the mean assay value of $I^{=} + 2I^{\perp}$ without competitors. F_{SB} is to be taken from the expression in eq 51. R_4 is a useful control parameter for assessing whether competitors that score well in R_1-R_3 systematically influence the total fluorescence intensity (*31*).

2. SIMULATIONS

In the second part of this paper, we will visually illustrate the key results obtained in the theroretical part. We will use physically realistic ranges for all parameters as they typically apply to FP assays. In all cases, L_{ST} was set to 30 nM (*31*). In general, L_{ST} needs to be much smaller than R_T, because otherwise excess amounts of free ligand would always be present, even without any added competitor. On the other hand, L_{ST} needs to be large enough to be detected at a good signal-to-noise ratio in the linear range of the fluorescence polarimeter (*18*, *31*). Simulations were carried out with Mathematica 4.1 (Wolfram Research, Champaign, IL) and SigmaPlot 2001 (SPSS, Chicago, IL).

2.1. Direct Binding. Characteristic, semilogarithmic direct binding curves without nonspecific effects ($N_S = 0$) are shown in Figure 2A. F_{SB} is depicted as a function of R_T for values of K_{D1} ranging from 0.01 to 1000 μM. Equation 9 was used. Nonspecific effects are illustrated in Figure 2B. K_{D1} was set to 1 μM, and binding curves are shown for N_S values ranging from 0 to 0.6. The axis on the right indicates the values of F_{SBA} (i.e., using the false assumption $N_S = 0$) for the blue curve, for which the true N_S is equal to 0.6. The corresponding value of K_{D1A} for the blue curve is 1.6 μM. Equations 9, 11, and 12 were used.

2.2. Complete Competitive Binding. Characteristic complete competitive binding curves without nonspecific effects ($N = 0$) are shown in Figure 3A. With both R_T and K_{D1} set equal to 1 μM, curves for values of K_{D2} ranging from 0.001 to 100 μM are depicted. Equation 17 was used. Note that with an increasing affinity of the competitor (i.e., decreasing K_{D2}) F_{SB} approaches zero when $L_T \approx R_T$, i.e., when total competitor and receptor concentrations are approximately equal. It is evident that accurate data fitting and estimation of K_{D2} become increasingly difficult for lower values of K_{D2}, since competition curves become more and more closely spaced. One way to address this limitation is to repeat the measurement at lower concentrations of R_T, which renders the assay more discriminatory for smaller values of K_{D2}.

Lowering R_T, however, concomitantly reduces the observed anisotropy in the absence of competitor, A_U, and thus the assay's signal-to-noise ratio. In practice, competitive binding of high-affinity ligands is best studied at the lowest R_T permitted by signal-to-noise considerations.

2.3. Incomplete Competitive Binding. Characteristic incomplete competitive binding curves without nonspecific effects ($N = 0$) are shown in Figure 3B. R_T and K_{D1} were set equal to 1 μM. K_{D2} equals 1 μM (red curves) or ranges from 0.1 to 10 μM (blue curves). K_{D3} ranges from 0.01 to 1000 μM. Equation 27 was used. The graphs illustrate the effects of the three independent dissociation constants, $K_{D1}-K_{D3}$. K_{D1} determines the value of F_{SB} when $L_T = 0$; K_{D2} shifts transition curves horizontally with respect to L_T, and K_{D3} specifies the asymptotic value of F_{SB} for large L_T values and, thereby, the degree of cooperativity or anticooperativity. When $K_{D2} = K_{D3}$, F_{SB} remains constant and independent of L_T. The asymptotic limits of F_{SB} for $L_T \rightarrow \infty$ depend on K_{D3} and are given by eq 28.

2.4. Relationship between FP Observables and Binding States. Figure 4A illustrates the effects of fluorescence intensity differences between bound and free labeled ligand (ratio expressed by Q) on observable anisotropy, A_{OBS}, in the direct binding model. For generality, A_{OBS} is shown normalized with respect to the difference between bound and free anisotropies, $A_B - A_F$. K_{D1} and N_S were set equal to 1 μM and 0, respectively. Q ranges from 0.1 to 10. Equations 9 and 39 were used. If it were (falsely) assumed for the blue curves that $Q = 1$, K_{D1} would be misestimated as 10.0200 $\pm$ 0.0014 μM ($Q = 0.1$, i.e., quenched fluorescence) and 0.0881 $\pm$ 0.0003 μM ($Q = 10$, i.e., enhanced fluorescence) by a nonlinear least-squares fit.

Figure 4B depicts the influence of Q on A_{OBS} for the case of complete competitive binding. R_T, K_{D1}, and K_{D2} were set to 1 μM ($N = 0$). Q ranges from 0.1 to 10. Equations 17 and 39 were used. If it were (falsely) assumed for the blue curves that $Q = 1$, one would obtain the following: $K_{D1} = 10.1300 \pm 0.0002$ μM and $K_{D2} = 1.0080 \pm 0.0002$ μM ($Q = 0.1$), or $K_{D1} = 0.0983 \pm 0.0001$ μM and $K_{D2} = 0.9947 \pm 0.0006$ μM ($Q = 10$) by a nonlinear least-squares fit. The noteworthy result is that, despite misestimation of K_{D1}, a correct estimation of K_{D2} is very insensitive to large errors in the estimate of Q. This finding is of great practical interest, since the ultimate goal of competitive binding assays is precisely the accurate characterization of competitor binding (K_{D2}), whereas the accuracy of the dissociation constant of the labeled probe (K_{D1}) is less significant.

2.5. Sensitivity of Competitive Binding Assays. Sensitivity-optimized values of F_{SB} at $L_T = 0$ are shown in Figure 5A as a function of K_{D2}. K_{D1} ranges from 0.1 to 10 μM. Equation 46 was used. The corresponding optimal values of R_T can be calculated from eq 43. For example, in our FP assay for inhibitors of the VIVIT−calcineurin interaction ($K_{D1} = 0.5$ μM, $L_{ST} = 30$ nM) (*31*), calcineurin concentrations of 0.52, 0.33, and 0.11 μM deliver optimal sensitivity for identifying small-molecule inhibitors with projected K_{D2} values of 100, 1, and 0.05 μM, respectively. The corresponding bound fractions of labeled VIVIT ligand (F_{SB}) are 0.50, 0.39, and 0.17, respectively. It is clear that the optimal sensitivity for high-affinity competitors is usually achieved when $F_{SB} < 0.5$.

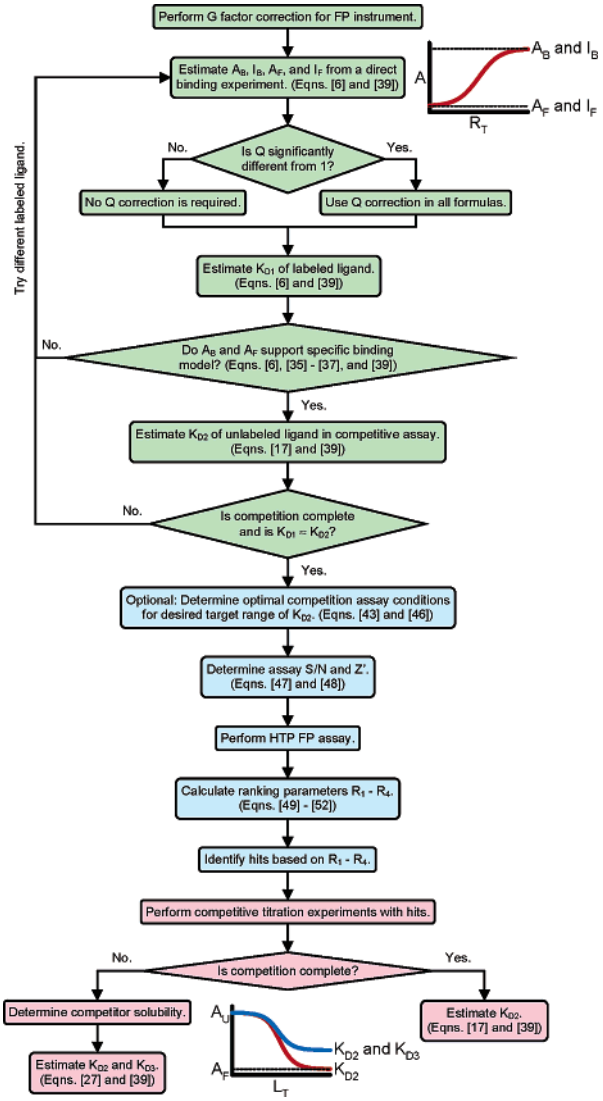

FIGURE 6: Procedural flowchart of a typical high-throughput (HTP) FP assay project. The color scheme highlights the three modules of the process: assay development (green), competitive HTP assay (blue), and follow-up titration data analysis (red). References to relevant equations in the text are given where appropriate.

Figure 5B depicts a two-dimensional contour plot, in which the normalized assay sensitivity, S/S_{MAX}, at $L_T = 0$ is graphed as a function of both F_{SB} and K_{D2} ($K_{D1} = 1$ μM). Equations 41 and 44 were used. Choices of parameter pairs that fall into the red or orange zones are favorable.

3. SUMMARY AND PROCEDURAL FLOWCHART

This paper develops a general theoretical framework for equilibrium binding experiments. Our only prior assumption was that thermodynamic ideality applies such that thermodynamic activities and concentrations are equivalent (*40*). All relationships are conveniently expressed in terms of *a priori* known total input concentrations. Exact algebraic relationships were derived for the determination of dissociation constants in competitive binding experiments.

A four-state model was introduced that can account for the frequently observed phenomenon of incomplete competitive dissociation. We showed that the neglect of potential nonspecific binding effects will, at worst, lead to overestimation of the respective dissociation constant, i.e., introduce a

conservative error corresponding to an upper bound estimate. Furthermore, we demonstrated that, even when the ratio Q of bound and free labeled ligand quantum quields is severely misestimated, an accurate estimation of the dissociation constant of the unlabeled competitor can nevertheless be obtained. These findings rationalize the great robustness of the competitive binding experimental design. Our sensitivity analysis provides guidance for the optimal choice of experimental parameters.

As a specific application, the theoretical framework was then linked to experimental observables as they occur in FP. Finally, scoring and ranking strategies were developed for application in high-throughput FP assays. Figure 6 lays out a procedural flowchart that summarizes the modular core elements of a competitive high-throughput FP screening effort, using the concepts developed in this paper. We shall point out that a very critical point for a successful screen is the careful choice of a labeled ligand. Its binding affinity for the receptor should be high, and the fluorophore should not be influenced by or interfere with the binding state; the fluorescence lifetime of the fluorophore needs to be appropriate, and nonspecific binding should be minimal. The subsequent paper (*31*) describes as a detailed practical example and application our experiences with the screening for small-molecule inhibitors of the protein−protein interaction between human calcineurin and NFAT (*31*).

SUPPORTING INFORMATION AVAILABLE

Derivation of key equations illustrated with Mathematica 4.1 (Wolfram Research, Champaign, IL). This material is available free of charge via the Internet at http://pubs.acs.org.

REFERENCES

1. Pawson, T., and Nash, P. (2000) Protein−protein interactions define specificity in signal transduction, *Genes Dev. 14*, 1027−1047.
2. Ashman, K., Moran, M. F., Sicheri, F., Pawson, T., and Tyers, M. (2001) Cell signalling: The proteomics of it all, *Sci. STKE 2001*, PE33.
3. Legrain, P., Wojcik, J., and Gauthier, J. M. (2001) Protein−protein interaction maps: A lead towards cellular functions, *Trends Genet. 17*, 346−352.
4. Tucker, C. L., Gera, J. F., and Uetz, P. (2001) Towards an understanding of complex protein networks, *Trends Cell Biol. 11*, 102−106.
5. Uetz, P. (2002) Two-hybrid arrays, *Curr. Opin. Chem. Biol. 6*, 57−62.
6. Uetz, P., Giot, L., Cagney, G., Mansfield, T. A., Judson, R. S., Knight, J. R., Lockshon, D., Narayan, V., Srinivasan, M., Pochart, P., Qureshi-Emili, A., Li, Y., Godwin, B., Conover, D., Kalbfleisch, T., Vijayadamodar, G., Yang, M., Johnston, M., Fields, S., and Rothberg, J. M. (2000) A comprehensive analysis of protein−protein interactions in *Saccharomyces cerevisiae*, *Nature 403*, 623−627.
7. Gavin, A. C., Bosche, M., Krause, R., Grandi, P., Marzioch, M., Bauer, A., Schultz, J., Rick, J. M., Michon, A. M., Cruciat, C. M., Remor, M., Hofert, C., Schelder, M., Brajenovic, M., Ruffner, H., Merino, A., Klein, K., Hudak, M., Dickson, D., Rudi, T., Gnau, V., Bauch, A., Bastuck, S., Huhse, B., Leutwein, C., Heurtier, M. A., Copley, R. R., Edelmann, A., Querfurth, E., Rybin, V., Drewes, G., Raida, M., Bouwmeester, T., Bork, P., Seraphin, B., Kuster, B., Neubauer, G., and Superti-Furga, G. (2002) Functional organization of the yeast proteome by systematic analysis of protein complexes, *Nature 415*, 141−147.
8. Boulton, S. J., Gartner, A., Reboul, J., Vaglio, P., Dyson, N., Hill, D. E., and Vidal, M. (2002) Combined functional genomic maps of the *C. elegans* DNA damage response, *Science 295*, 127−131.
9. Jones, S., and Thornton, J. M. (1996) Principles of protein−protein interactions, *Proc. Natl. Acad. Sci. U.S.A. 93*, 13−20.
10. Lo Conte, L., Chothia, C., and Janin, J. (1999) The atomic structure of protein−protein recognition sites, *J. Mol. Biol. 285*, 2177−2198.
11. Peczuh, M. W., and Hamilton, A. D. (2000) Peptide and protein recognition by designed molecules, *Chem. Rev. 100*, 2479−2494.
12. Cochran, A. G. (2000) Antagonists of protein−protein interactions, *Chem. Biol. 7*, R85−R94.
13. Cox, B., Denyer, J. C., Binnie, A., Donnelly, M. C., Evans, B., Green, D. V., Lewis, J. A., Mander, T. H., Merritt, A. T., Valler, M. J., and Watson, S. P. (2000) Application of high-throughput screening techniques to drug discovery, *Prog. Med. Chem. 37*, 83−133.
14. Hertzberg, R. P., and Pope, A. J. (2000) High-throughput screening: New technology for the 21st century, *Curr. Opin. Chem. Biol. 4*, 445−451.
15. Sittampalam, G. S., Kahl, S. D., and Janzen, W. P. (1997) High-throughput screening: Advances in assay technologies, *Curr. Opin. Chem. Biol. 1*, 384−391.
16. Toogood, P. L. (2002) Inhibition of protein−protein association by small molecules: Approaches and progress, *J. Med. Chem. 45*, 1543−1558.
17. Strausberg, R. L., and Schreiber, S. L. (2003) From knowing to controlling: A path from genomics to drugs using small molecule probes, *Science 300*, 294−295.
18. Roehrl, M. H. A., Kang, S., Aramburu, J., Wagner, G., Rao, A., and Hogan, P. G. (2004) Selective inhibition of calcineurin-NFAT signaling by blocking protein−protein interaction with small organic molecules, *Proc. Natl. Acad. Sci. U.S.A. 101*, 7554−7559.
19. Pope, A. J., Haupts, U. M., and Moore, K. J. (1999) Homogeneous fluorescence readouts for miniaturized high-throughput screening: Theory and practice, *Drug Discovery Today 4*, 350−362.
20. Jameson, D. M., and Seifried, S. E. (1999) Quantification of protein−protein interactions using fluorescence polarization, *Methods 19*, 222−233.
21. Tetin, S. Y., and Hazlett, T. L. (2000) Optical spectroscopy in studies of antibody-hapten interactions, *Methods 20*, 341−361.
22. Weber, G. (1951) Polarization of the fluorescence of macromolecules. 1. Theory and experimental method, *Biochem. J. 51*, 145−155.
23. Levine, L. M., Michener, M. L., Toth, M. V., and Holwerda, B. C. (1997) Measurement of specific protease activity utilizing fluorescence polarization, *Anal. Biochem. 247*, 83−88.
24. Zhang, H., Nimmer, P., Rosenberg, S. H., Ng, S. C., and Joseph, M. (2002) Development of a high-throughput fluorescence polarization assay for Bcl-x(L), *Anal. Biochem. 307*, 70−75.
25. Cantor, C. R., and Schimmel, P. R. (1980) *Biophysical Chemistry*, Freeman, New York.
26. Fersht, A. (1999) *Structure and Mechanism in Protein Science*, Freeman, New York.
27. Creighton, T. E. (1993) *Proteins: Structures and Molecular Properties*, 2nd ed., Freeman, New York.
28. Voet, D., and Voet, J. G. (1990) *Biochemistry*, Wiley, New York.
29. Kuzmic, P. (1999) General numerical treatment of competitive binding kinetics: Application to thrombin-dehydrothrombin-hirudin, *Anal. Biochem. 267*, 17−23.
30. Wang, Z. X. (1995) An exact mathematical expression for describing competitive binding of two different ligands to a protein molecule, *FEBS Lett. 360*, 111−114.
31. Roehrl, M. H. A., Wang, J. Y., and Wagner, G. (2004) Disovery of small-molecule inhibitors of the NFAT-calcineurin interaction by competitive high-throughput fluorescence polarization screening, *Biochemistry 43*, 16067−16075.
32. Roehrl, M. H. A. Unpublished data.
33. Cantor, C. R., and Schimmel, P. R. (1980) in *Biophysical Chemistry*, pp 409−480, Freeman, New York.
34. Cantor, C. R., and Schimmel, P. R. (1980) in *Biophysical Chemistry*, pp 562−565, Freeman, New York.
35. Garcia De La Torre, J., Huertas, M. L., and Carrasco, B. (2000) Calculation of hydrodynamic properties of globular proteins from their atomic-level structure, *Biophys. J. 78*, 719−730.
36. Allen, M., Reeves, J., and Mellor, G. (2000) High throughput fluorescence polarization: A homogeneous alternative to radioligand binding for cell surface receptors, *J. Biomol. Screening 5*, 63−69.

37. Parker, G. J., Law, T. L., Lenoch, F. J., and Bolger, R. E. (2000) Development of high throughput screening assays using fluorescence polarization: Nuclear receptor−ligand-binding and kinase/phosphatase assays, *J. Biomol. Screening 5*, 77−88.

38. Dandliker, W. B., Hsu, M.-L., Levin, J., and Rao, B. R. (1981) in *Methods in Enzymology* (Langone, J., and Van Vunakis, H., Eds.) pp 3−28, Academic Press, New York.

39. Zhang, J. H., Chung, T. D., and Oldenburg, K. R. (1999) A simple statistical parameter for use in evaluation and validation of high throughput screening assays, *J. Biomol. Screening 4*, 67−73.

40. Tinoco, I., Sauer, K., and Wang, J. C. (1995) in *Physical Chemistry: Principles and Applications in Biological Sciences*, pp 123−194, Prentice-Hall, Englewood Cliffs, NJ.

BI048233G